

PSU/TH/190

# Probing small- $x$ parton densities in proton-proton (-nucleus) collisions in the very forward direction

Lyndon Alvero, John C. Collins, Mark Strikman, and J.J. Whitmore

*Physics Department, 104 Davey Lab, Pennsylvania State University, University Park, PA 16802-6300, U.S.A.*  
(27 October 1997)

## Abstract

We present calculations of several  $pp$  scattering cross sections with potential applications at the LHC. Significantly large rates for momentum fraction,  $x$ , as low as  $10^{-7}$  are obtained, allowing for possible extraction of quark and gluon densities in the proton and nuclei down to these small  $x$  values provided a detector with good acceptance at maximal rapidities is used.

PACS number(s): 12.38.Bx, 13.85.-t, 13.87.-a, 13.90.+i

## I. INTRODUCTION

In this paper, we study the measurement of quark and gluon distribution functions inside the proton at very small momentum fractions  $x$ . We consider several processes in  $pp$  collisions at a center-of-mass energy ( $\sqrt{s}$ ) of 14 TeV and show that the range of useful measurements extends down to about  $x \sim 10^{-6}$  for most processes, and even down to  $x \sim 10^{-7}$  for the Drell-Yan process.<sup>1</sup> Such measurements require a detector which has sufficient acceptance at maximal rapidities. Plans for building a detector of this type (FELIX) are under discussion at the LHC [1]. We show how the parton densities may be determined. The event rates are high; to estimate them, we use the CTEQ3M distributions [2] to provide an extrapolation from the region where measurements currently exist, which is  $x \geq 10^{-4}$ .

Although our results are obtained for proton-proton interactions, a similar analysis can easily be applied to proton-nucleus interactions in the same accelerator. For example, in the case of proton-calcium collisions, at say a center-of-mass energy of 63 TeV, the same region, down to  $x \sim 10^{-6}$  and lower, can also be probed. We show how data from such studies would provide information on the parton densities in nuclei at both large and small  $x$ . Previous data for hard processes on nuclei have been confined to fixed-target energies, and so the range of processes for which perturbative QCD (pQCD) calculations are reliable is limited.

At the LHC, the integrated luminosity for a proton-proton luminosity of  $10^{31} \text{ cm}^{-2} \text{ s}^{-1}$  and a run-time of  $10^7 \text{ sec/yr}$  is  $100 \text{ pb}^{-1}$ . However, there is a loss of luminosity in proton-nucleus collisions; for protons on calcium, a luminosity of  $10^{30} \text{ cm}^{-2} \text{ s}^{-1}$  with a shorter running time is envisaged. This loss of luminosity is to a large extent compensated by increased cross sections, which are approximately proportional to the mass number  $A$  for large  $x$ . At small  $x$ , the cross sections presumably behave more like  $A^{2/3}$ , but as we will see, the event rates are so large that the resulting loss of event-rate relative to proton-proton collisions will still enable a lot of physics to be probed.

## II. KINEMATICS AND CROSS SECTIONS

We consider the following hadronic processes at center of mass energy  $\sqrt{s} = 14 \text{ TeV}$  with  $s = (p_1 + p_2)^2$

$$\begin{aligned}
p(p_1) + p(p_2) &\rightarrow \text{jet} + \gamma + \text{X} & (\text{J}\gamma), \\
p(p_1) + p(p_2) &\rightarrow l\bar{l} + \text{X} & (\text{DY}), \\
p(p_1) + p(p_2) &\rightarrow \text{jet}_1 + \text{jet}_2 + \text{X} & (\text{JJ}), \\
p(p_1) + p(p_2) &\rightarrow Q + \bar{Q} + \text{X} & (\text{HQ}), \\
p(p_1) + p(p_2) &\rightarrow W/Z + \text{X} & (\text{VB}),
\end{aligned} \tag{1}$$

where  $\gamma$  denotes a photon,  $l\bar{l}$  a lepton pair,  $Q(\bar{Q})$  a heavy quark (antiquark) and  $W, Z$  are the weak vector-bosons.

---

<sup>1</sup>Similar considerations are valid for the Tevatron collider where due to the smaller  $\sqrt{s}$  the relevant regions in  $x$  are scaled up by a factor of  $\sim 60$ .

To calculate the cross sections, we use the pQCD formalism, with the lowest-order hard scattering cross sections found, for example, in Refs. []. For the production of jets, photons and heavy quarks, we impose a cut  $p_{T,\min} = 10 \text{ GeV}$ , which will keep us in the region where perturbative calculations are applicable. Since our main interest is to probe parton densities at small  $x$ , we will mostly need asymmetric configurations of the momentum fractions,  $x_1$  and  $x_2$ , of the partons entering the hard scattering. From the kinematic inequality

$$x_1 x_2 \geq \frac{4p_{T,\min}^2}{s},$$

we deduce that the momentum fractions obey  $x_1 x_2 \geq 2 \times 10^{-6}$ . High-energy data on soft hadron production indicate [] that for fixed  $y_{\max} - y$ , where  $y$  is the particle rapidity, the soft hadronic multiplicity does not increase with energy, although at  $y = 0$  it grows rapidly with  $s$ . Thus, for the large values of  $y$  that we use in this analysis, soft interactions result in much smaller underlying event  $E_T$  pedestals than for  $y \sim 0$  at LHC energies. Moreover, for  $x$  substantially larger than  $x_{\min} = 2 \times 10^{-6}/\max(x_1, x_2)$ , the counting rates are so high for moderate  $p_T$  of the jets (in processes  $J\gamma$  and  $JJ$  in expression (1)) that it would be possible to restrict the analysis to the region of sufficiently large  $x$  (for one of the partons) so that the jets are still produced at large  $y$ . Indeed, the expected rates are so high that it would be also possible to check the role of the pedestals by taking data at several  $x$  bins. Hence, our choice of  $p_{T,\min} = 10 \text{ GeV}$  appears safe.

Since our interest is only in estimating rates and not in a detailed extraction of parton densities from data, it will be sufficient to perform leading-order calculations for most of the processes considered. Of course, when actual data become available, it will be necessary to fit the parton densities to the data with the aid of theoretical formulae at the best possible accuracy, at least next-to-leading order.

At small  $x$ , the gluon density is substantially larger than the quark densities. Since at lowest order, the Drell-Yan and vector-boson processes are given by quark-antiquark annihilation, without a gluon-induced subprocess, we will calculate these processes to next-to-leading order, with the hard-scattering coefficients in the  $\overline{\text{MS}}$  scheme found in Ref. [].

For jet, photon and heavy-quark production, we will set the renormalization and factorization scale  $\mu$  to the commonly used value of  $p_T$ . For Drell-Yan and vector-boson production, we set  $\mu$  to the pair mass and vector-boson mass, respectively.

### III. JET PLUS PHOTON

We calculate the cross section for producing a jet and a photon, putting the events in bins of  $p_T$  and  $x$ , where  $x$  is the minimum of the momentum fractions,  $x_1$  and  $x_2$ , of the incoming partons. The  $x$  bin is defined by  $x/\Delta \leq x \leq x\Delta$ , where  $\Delta = 10^{\frac{1}{2n_{div}}}$  with  $n_{div} = 10$ , while the bin size in  $p_T$  is set to 20% of the central value up to  $p_T \sim 110 \text{ GeV}$  and 40% beyond this  $p_T$  value. These same bin sizes are also used in the other cross sections computed in this paper.

The cross sections shown in Fig. 1 correspond to the kinematic region

$$(x_1 \ll x_2 \leq 0.8) \cup (x_2 \ll x_1 \leq 0.8). \quad (2)$$

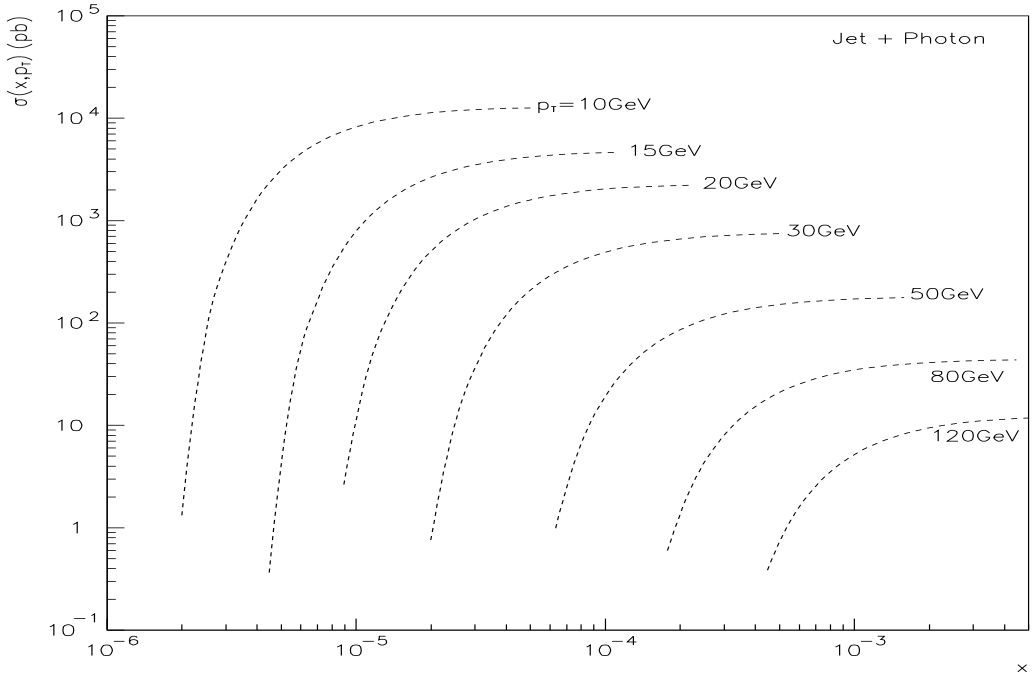


FIG. 1. The cross section  $\sigma(x, p_T)$  for Jet +  $\gamma$  production as a function of  $x = \min(x_1, x_2)$  and  $p_T$ . It is integrated over a  $p_T$  bin which is 20-40% of the central value (see text),  $\max(x_1, x_2) < 0.8$  and  $x/\Delta < \min(x_1, x_2) < x\Delta$ , where  $\Delta = 10^{1/20}$ . This choice of  $\Delta$  corresponds to 10 bins per decade in  $x$ .

One sees that large cross sections (above 10 pb) are obtained for  $p_T$  up to about 100 GeV. Combined with a luminosity of  $100 \text{ pb}^{-1}/\text{yr}$ , this gives at least hundreds of events in every bin, which will give good statistical precision. The strong fall-off of the curves at their left end is a result of approaching the kinematic limit:  $x > 4p_{T,\min}^2/s$ . To get a useful number of events, it is sufficient for  $x$  to be about twice its limit.

The cross section is dominated by gluon-quark scattering. In Fig. 2, the cross section integrated over  $p_T > 10 \text{ GeV}$  is split into  $gq$  and  $q\bar{q}$  components, and we see that the  $gq$  term is about an order of magnitude larger over the whole range shown. As before, the fall-off at the left is a consequence of the chosen minimum  $p_T$ . Since the incoming quark is typically at large  $x$ , where its distribution is already known fairly accurately [], photon-jet production provides a direct measurement of the gluon density for small  $x$  in the range  $x > 2.5 \times 10^{-6}$ .

To illustrate the accuracy that can be achieved in a determination of the gluon density, we show in Fig. 3 the CTEQ3M gluon momentum density  $xG(x, Q^2 = p_T^2)$  together with the statistical errors on measurements that correspond to the cross sections in Fig. 1. Notice that there is sufficient precision not merely to measure the gluon density but also to test its evolution. The cross sections presented here are, of course, the result of an extrapolation of parton densities from a region where they have been measured to much smaller  $x$  values.

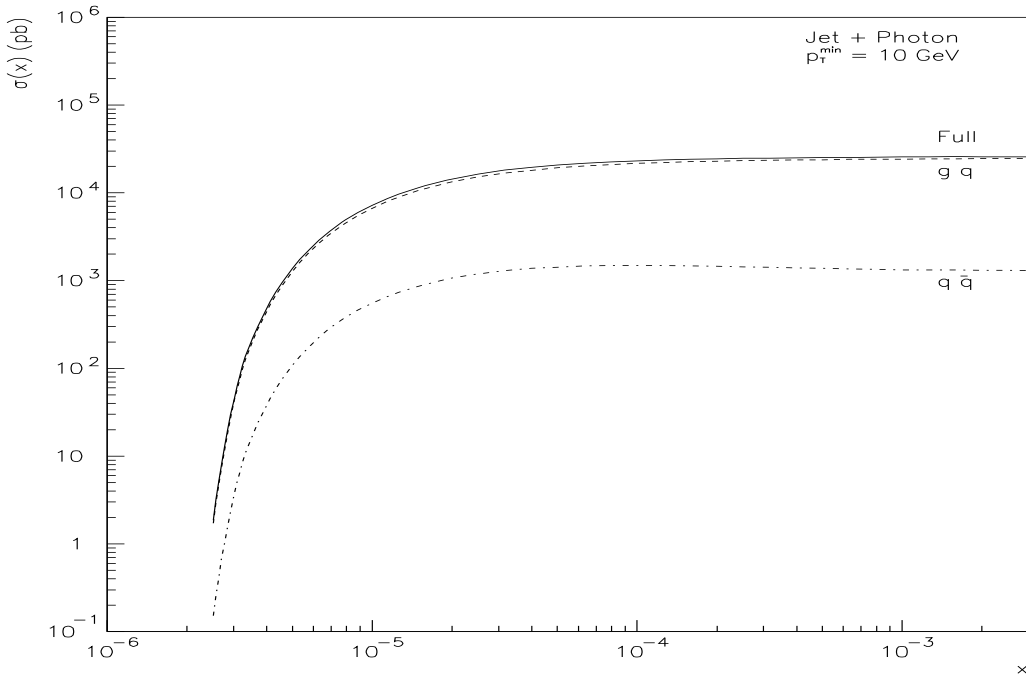


FIG. 2. The cross section  $\sigma(x)$  for Jet +  $\gamma$  production as a function of  $x = \min(x_1, x_2)$ . It is integrated over  $p_T > 10$  GeV and the same region in  $x_1, x_2$  as in the caption for Fig. 1.

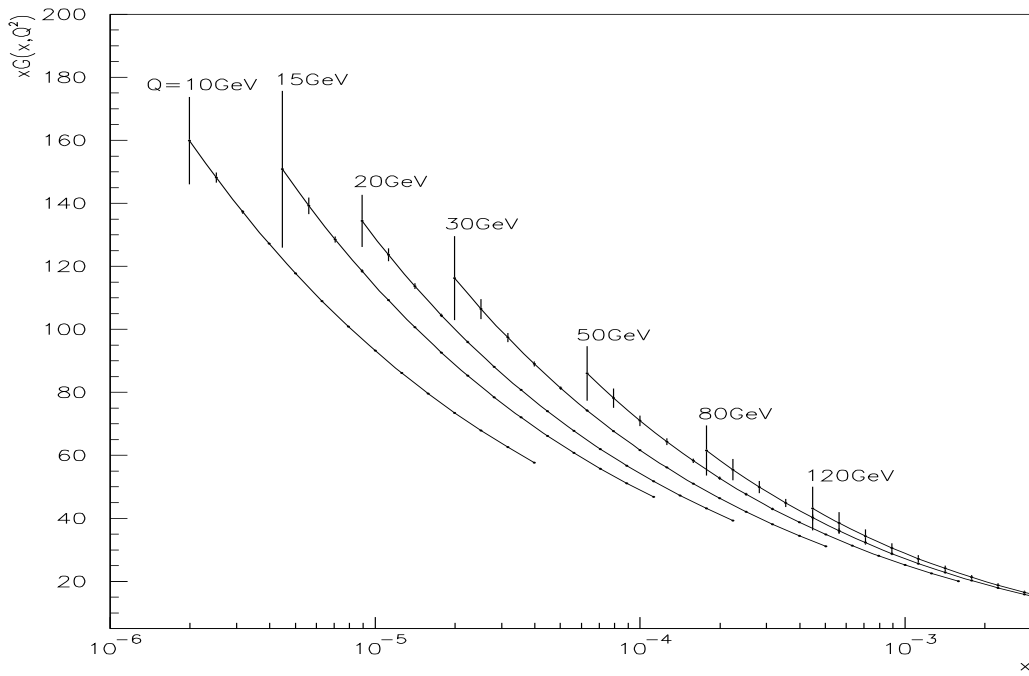


FIG. 3. The gluon momentum distribution with error bars calculated from the Jet +  $\gamma$  cross section and a data sample corresponding to an integrated luminosity of  $100 \text{ pb}^{-1}$ .

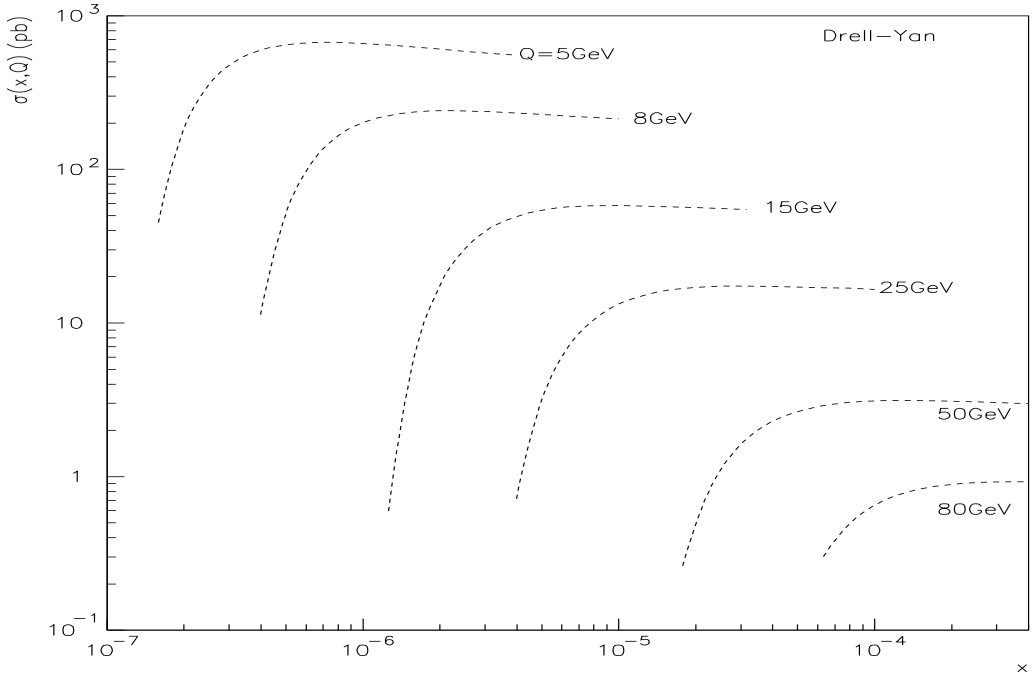


FIG. 4. The cross section  $\sigma(x, Q)$  for Drell-Yan as a function of  $x = \min(x_1, x_2)$  and  $Q$ . It is integrated over a  $Q$  bin which is 20-40% of the central value and the same region in  $x_1, x_2$  as in the caption for Fig. 1.

#### IV. LEPTON PAIRS

We next consider lepton pair production from hadrons (the Drell-Yan process). Using the same kinematic region defined by expression (2), we obtain the next-to-leading order cross sections shown in Fig. 4. Again, the relatively large cross sections lead to a large number of events expected at the LHC. More significantly, by measuring cross sections at smaller values of the pair mass  $Q$ , we can obtain parton densities at lower values of  $x$  than in the other processes considered in this paper. The advantage of the Drell-Yan process is that one can go to fairly small  $Q$  values while still trusting the pQCD formalism.

The dominant contribution for this process comes from the  $u\bar{u}$  channel; the  $qg$  contributions are about 30 times smaller than those from  $q\bar{q}$ . Using quark distributions  $q(x_2)$  which are well-determined for large  $x_2$ , one may then extract antiquark densities  $\bar{q}(x)$  at small  $x$ . We show in Fig. 5 a plot of the extrapolated CTEQ3M antiquark density  $x\bar{u}(x, Q^2)$  with the statistical errors based on the cross sections shown in Fig. 4. Note that we consider the Drell-Yan process down to relatively small pair masses  $\sim 5$  GeV. This assumes that, in the experiment, the detector will be able to suppress the background due to heavy flavor decays. Such suppression might be achieved using information from the forward calorimeters as well as from microvertex detectors.

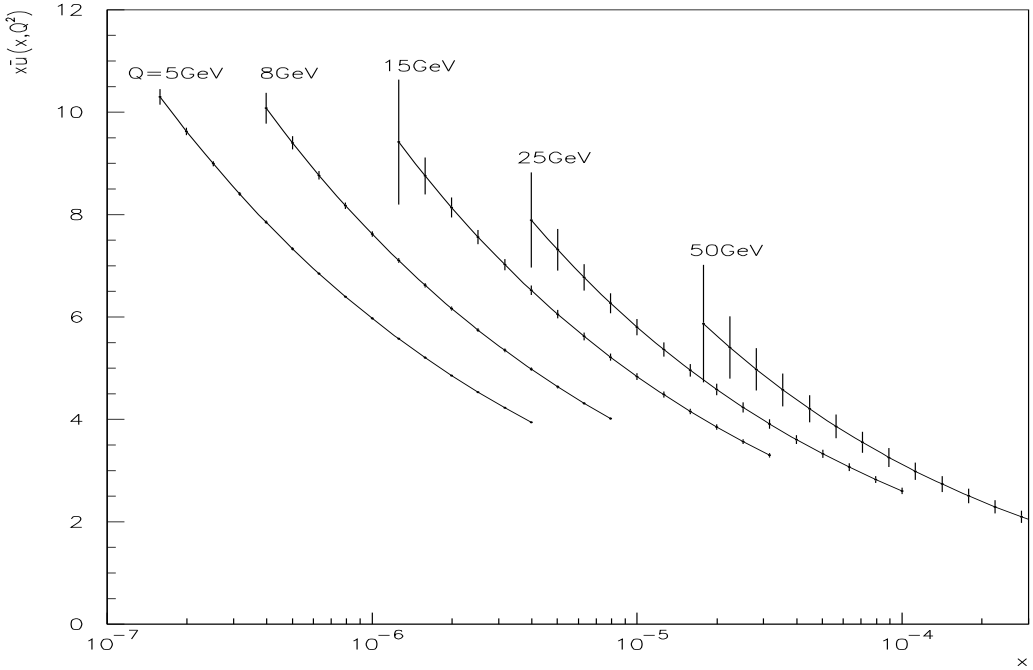


FIG. 5. The  $\bar{u}$  antiquark momentum distribution with error bars calculated from the Drell-Yan cross section and a data sample corresponding to an integrated luminosity of  $100 \text{ pb}^{-1}$ .

## V. TWO JETS

We next consider the cross section for the production of dijets. Fig. 6 shows the cross section in bins of  $p_T$  and  $x$ , in the region defined by expression (2). The cross sections obtained are about 100 times larger than all the others computed in this paper.

In Fig. 7, we show the  $x$  distribution of the cross section. Aside from the total cross section (solid curve), we also exhibit the contributions from the different partonic channels:  $gg$  (dashed),  $gq$  (upper dotted),  $qq$  (lower dotted) and  $q\bar{q}$  (dot-dashed curve). The largest contributions to the cross section come from the  $gg$  and  $gq$  channels. This process thus provides an independent consistency check of the parton distributions, primarily the gluon density, obtained from other processes.

## VI. $W$ PRODUCTION

Production of  $W$ -bosons in the forward direction provides a complementary way to measure sea quark distributions at small  $x$ . At the same time, comparison of the rates of production of  $W^+$  and  $W^-$  bosons would provide a new method to measure the ratio  $r(x, Q^2) = \frac{u(x, Q^2)}{d(x, Q^2)}$  at large  $x$  [1]. (Such a measurement would rely on the presumed equality of  $\bar{u}$  and  $\bar{d}$  distributions at small  $x$ .) Current determinations of  $u/d$  rely on data from deuterium targets, where nuclear effects can be large for  $x \geq 0.5$ . Notice that most of the current global fits, eg. [1], assume that  $r \rightarrow 0$  when  $x \rightarrow 1$ , whereas a perturbative QCD

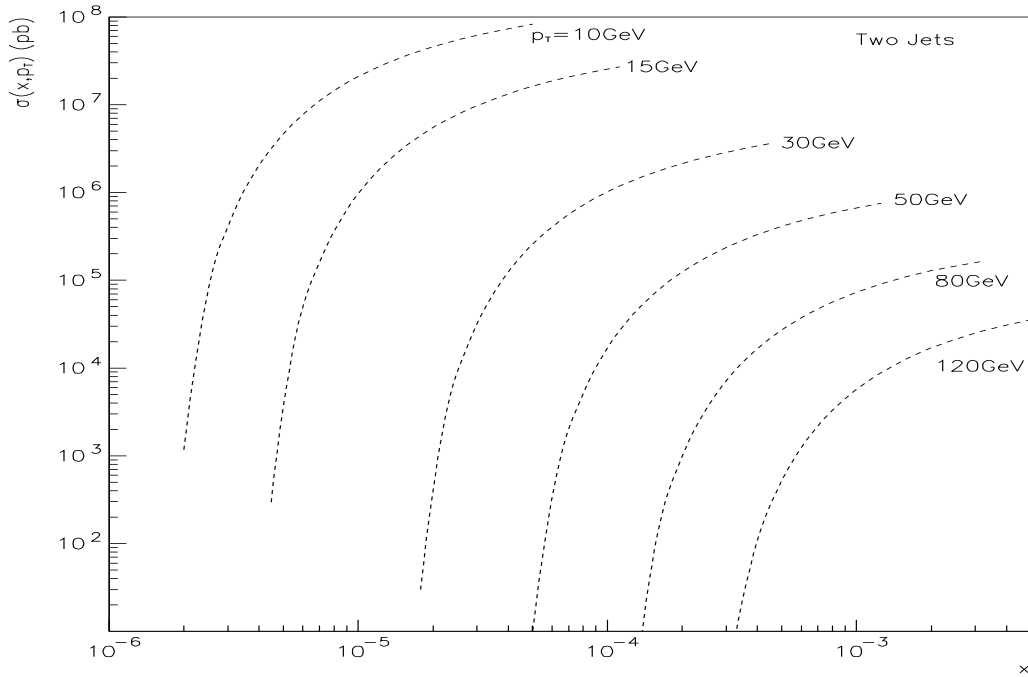


FIG. 6. The cross section  $\sigma(x, p_T)$  for dijet production as a function of  $x = \min(x_1, x_2)$  and  $p_T$ . Same comments as in the caption for Fig. 1 apply.

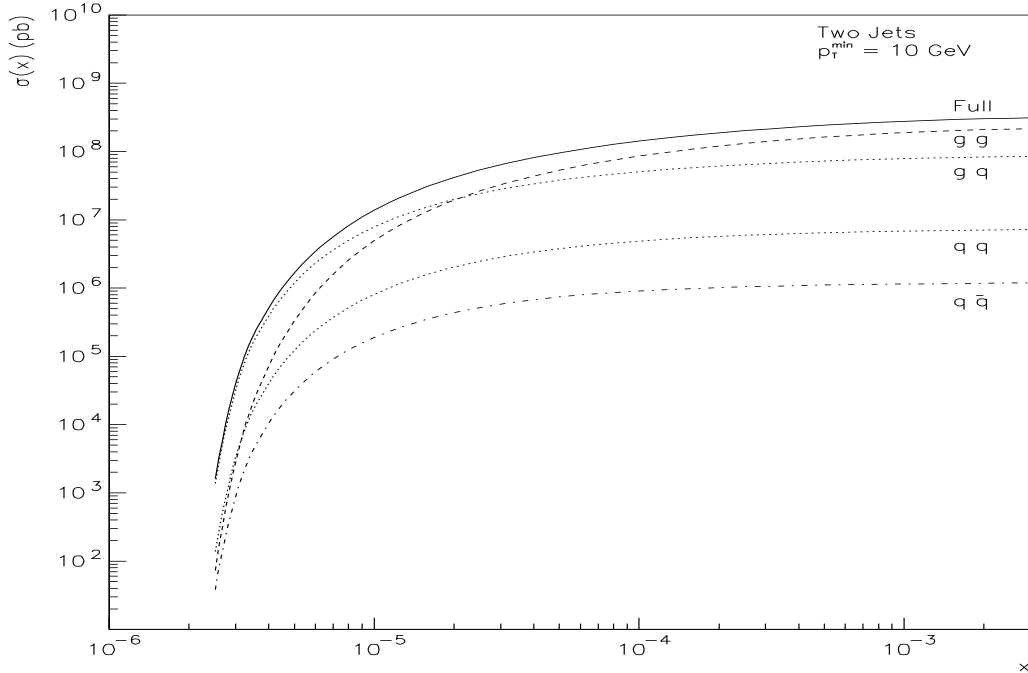


FIG. 7. The cross section  $\sigma(x)$  for dijet production as a function of  $x = \min(x_1, x_2)$ . Same comments as in the caption for Fig. 2 apply.

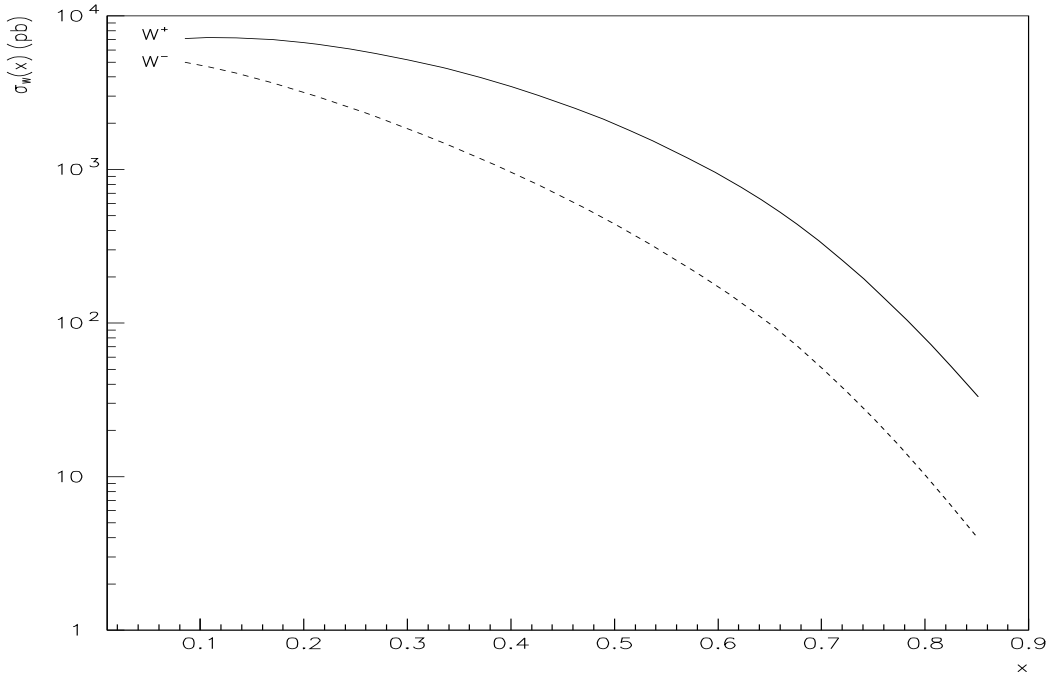


FIG. 8. The cross section  $\sigma(x)$  for  $W$  production as a function of  $x = x_1$ . It is integrated over  $x/\Delta < x < x\Delta$ , where  $\Delta = 10^{1/20}$ . This choice of  $\Delta$  corresponds to 10 bins per decade in  $x$ . Note that for this process,  $x_2 = M_W^2/(xs)$ .

analysis of the leading diagrams for the  $x \rightarrow 1$  limit [] suggests that  $r \rightarrow 0.2$  in this limit. A direct measurement independent of any data requiring knowledge of nuclear effects would be valuable.

At next-to-leading order, we calculate the cross sections for  $W^+$  and  $W^-$  production in bins of  $x$ . One observes from Fig. 8 that significant rates can be measured up to  $x \sim 0.8$ . This implies that quark distributions at  $Q^2 \sim 10^4$  GeV $^2$  can be measured from the sum of the cross sections for production of  $W^+$  and  $W^-$ -bosons down to  $x \sim 5 \times 10^{-5}$ . At the same time, one would be able to distinguish between different scenarios for the asymptotic behaviour of the  $u/d$  ratio in the  $x \rightarrow 1$  limit.

## VII. HEAVY QUARKS

We show in Figs. 9 and 10 the  $(x, p_T)$  and  $x$  distributions, respectively, for charm quark production in the region defined by expression (2). The same general features as in the plots for jet plus photon and dijets are observed.

In Fig. 10, the contributions from the two active partonic channels are also shown:  $gg$  (dashed curve) and  $q\bar{q}$  (dot-dashed curve). The total cross section is of order 1 to  $10^2$  pb when  $2.5 \times 10^{-6} \leq x \leq 4 \times 10^{-6}$ . In this region, the  $q\bar{q}$  contribution dominates, being about 10 times larger than that of the  $gg$  channel. In the region  $10^{-4} \leq x \leq 10^{-3}$ , the total cross section rises, is of order  $10^5$  pb and mostly consists of  $gg$  channel contributions; the  $q\bar{q}$  contribution drops to about 10% of the total.

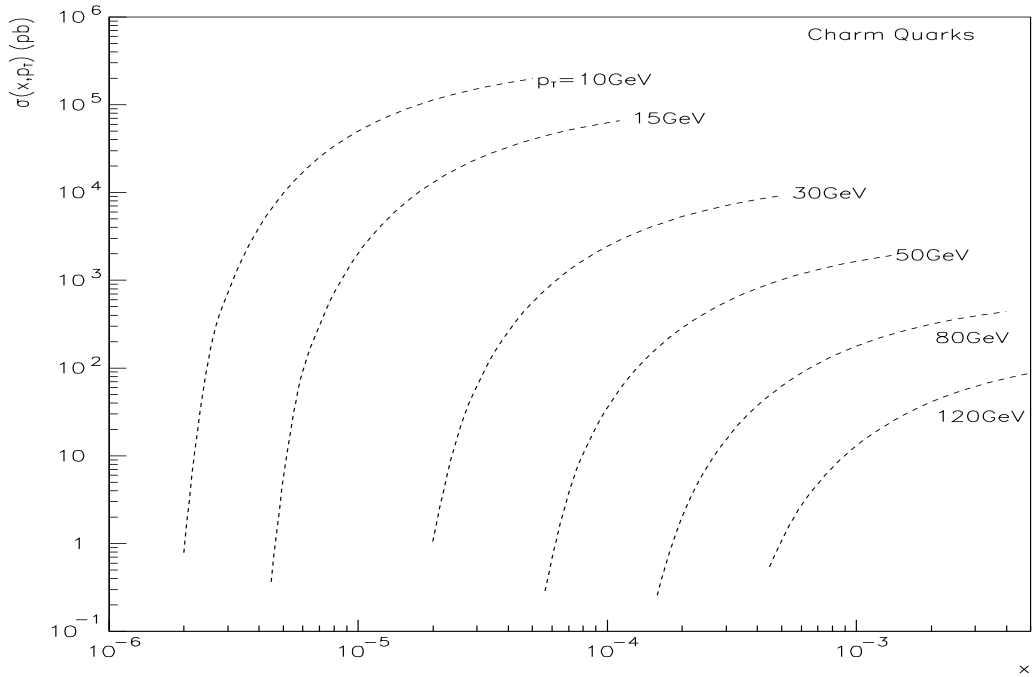


FIG. 9. The cross section  $\sigma(x, p_T)$  for charm quark production as a function of  $x = \min(x_1, x_2)$  and  $p_T$ . Same comments as in the caption for Fig. 1 apply.

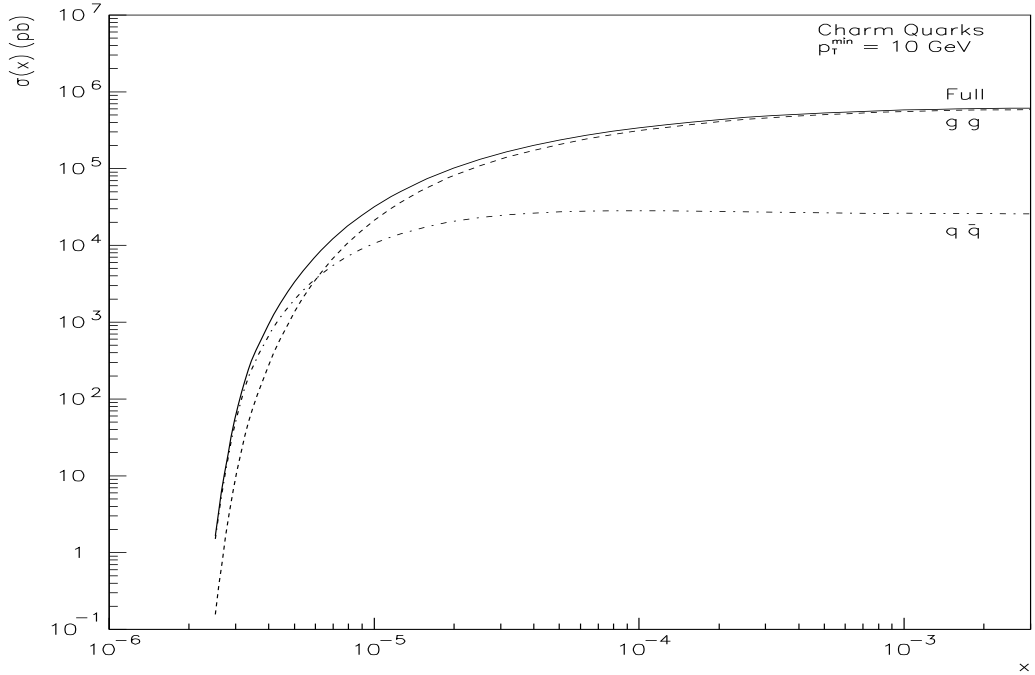


FIG. 10. The cross section  $\sigma(x)$  for charm quark production as a function of  $x = \min(x_1, x_2)$ . Same comments as in the caption for Fig. 2 apply.

Thus, it is possible to extract the antiquark (or quark) density at  $x \sim 3-4 \times 10^{-6}$  from the charm quark cross section providing a cross-check of the antiquark densities obtained from Drell-Yan measurements. In this case, the background consisting of  $gg$  channel contributions is well determined with the use of the gluon density obtained from the jet plus photon or dijet cross section as described in Sections III and V. Similarly, it is also possible to extract the gluon density at  $x \geq 10^{-4}$  from this type of cross section, providing a cross-check of gluon densities derived from other measurements.

### VIII. CONCLUSIONS

We have shown, in several independent ways, how parton distributions in nucleons and nuclei (nuclear shadowing) down to  $x \sim 10^{-7}$  may be measured from hadron-hadron interactions at LHC energies. In particular, we show in Figs. 11 and 12 the regions in energy  $E = (p_T, Q \text{ or } M_W)$  and momentum fraction  $x$  where measurements can be made for extracting antiquark and gluon densities, respectively, at better than 20% accuracy from the different hadronic processes considered, assuming an integrated luminosity of  $100 \text{ pb}^{-1}$ .

In Fig. 11, the region marked with cross-hatch shading shows where the Drell-Yan process determines the antiquark densities with better than 20% accuracy. The dashed horizontal line is where  $W$  production determines these densities. The small triangle with horizontal shading shows where charm production determines the antiquark densities. The dotted curve shows the minimum value of  $x$  as a function of the pair mass  $Q$  in the Drell-Yan process.

Similarly, we show in Fig. 12 the regions where data on the different processes can determine the gluon density. The regions marked with vertical, horizontal and slanted lines correspond to jet plus photon, charm quark and dijet production, respectively. The dot-dashed curve represents the minimum allowed value of  $x$  as a function of the  $p_T$  of the jet or heavy quark.

In our calculations, we have assumed that the usual DGLAP evolution equations apply to the parton densities in the very small  $x$  region being considered and that CTEQ3M parton distributions can be extrapolated outside the region in which they are valid. However, it may well be that other physics effects, notably gluon recombination [], are important at these small  $x$  values. As we have seen, by measuring parton densities over a wide range of scales and in several processes, one can, in fact, test whether DGLAP evolution and the rest of the factorization method is valid — see, for example, Figs. 3 and 5. Of course, if the measurements fail consistency checks, for example if DGLAP evolution is found to fail, then one can no longer say that it is the parton densities that are being measured, but rather that one is probing new effects at small  $x$ .

### ACKNOWLEDGMENTS

This work was supported in part by the U.S. Department of Energy under grant numbers DE-FG02-90ER-40577 and DE-FG02-93ER40771 and by the U.S. National Science Foundation.

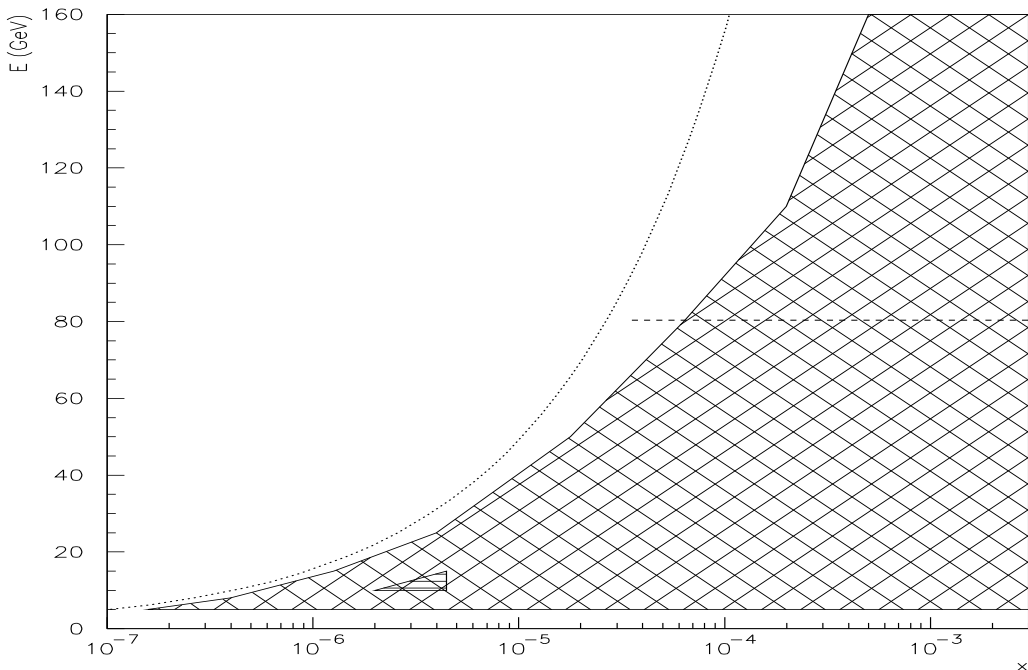


FIG. 11. A contour plot showing the region in  $(E, x)$  where measurements of the antiquark densities in the proton can be made to within 20% accuracy, assuming an integrated luminosity of  $100 \text{ pb}^{-1}$ . The region marked with cross-hatch shading corresponds to the Drell-Yan process. The dashed horizontal line is where  $W$  production dominates. The dotted curve shows the minimum value of  $x$  as a function of the pair mass in the Drell-Yan process. The small triangle with horizontal shading shows where charm production is dominated by the  $q\bar{q} \rightarrow c\bar{c}$  subprocess.

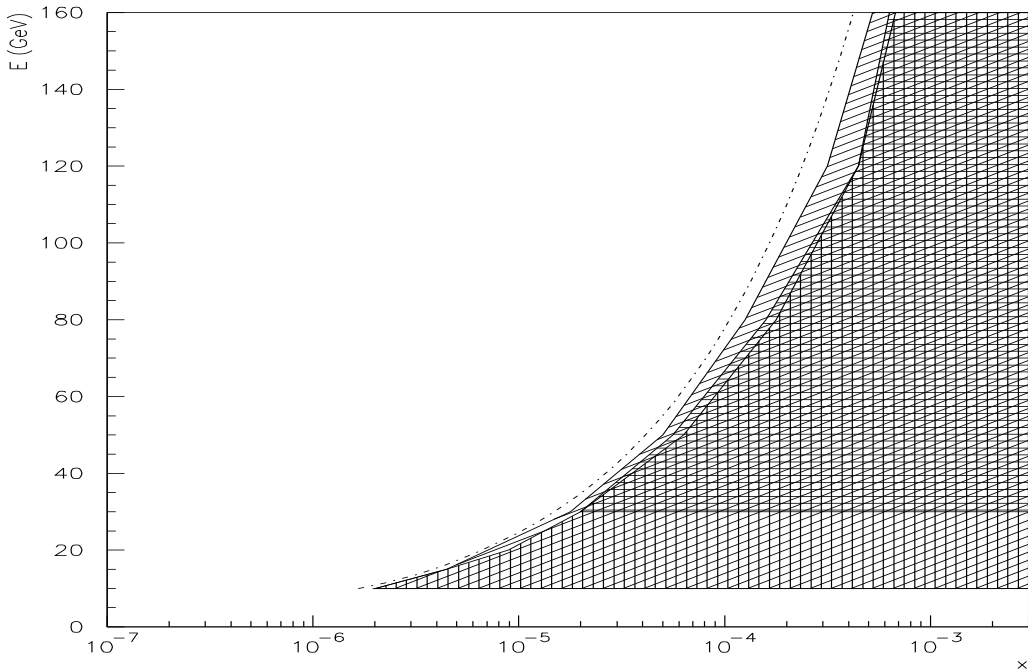


FIG. 12. A contour plot showing the region  $(E, x)$  where measurements of the gluon density in the proton can be made to within 20% accuracy, assuming an integrated luminosity of  $100 \text{ pb}^{-1}$ . The dot-dashed curve represents the minimum allowed value of  $x$  as a function of the  $p_T$  of the jet or heavy quark. The regions marked with vertical, horizontal and slanted lines correspond to jet plus  $\gamma$ , charm quark and dijet production, respectively.

## REFERENCES

- [1] FELIX Collaboration, “FELIX: A Full Acceptance Detector at the LHC”, CERN/LHCC 97-45. Also accessible on the internet: <http://www.cern.ch/FELIX/Loi/loi.html>.
- [2] H. L. Lai et al., Phys. Rev. D **51** (1995) 4763. The CTEQ parton distributions can be obtained from <http://www.phys.psu.edu/~cteq/>.
- [3] G. Sterman et al. (CTEQ Collaboration), “Handbook of perturbative QCD”, Rev. Mod. Phys. **67** (1995) 157.
- [4] E. Eichten, I. Hinchliffe, K. Lane and C. Quigg, Rev. Mod. Phys. **56** (1984) 579; **58** (1986) 1065.
- [5] G. J. Alner et al. (UA5 collaboration), Phys. Rep. **154** (1987) 247.
- [6] R. Hamberg, W. L. van Neerven and T. Matsuura, Nucl. Phys. B **359** (1991) 343.
- [7] W. Melnitchouk and J. C. Peng, Phys. Lett. B **400** (1997) 220;  
E. L. Berger, F. Halzen, C. S. Kim and S. Willenbrock, Phys. Rev. D **40** (1989) 83.
- [8] G. R. Farrar and D. R. Jackson, Phys. Rev. Lett. **35** (1975) 1416.
- [9] A. H. Mueller and Jianwei Qiu, Nucl. Phys. B **268** (1986) 427.